IET Microwaves, Antennas & Propagation

Research Article

IET Journals
The Institution of Engineering and Technology

New technique for shaping axisymmetric dual-reflector antennas using conic sections to control aperture illumination

ISSN 1751-8725
Received on 13th February 2020
Revised 9th May 2020
Accepted on 9th July 2020
doi: 10.1049/iet-map.2020.0156
www.ietdl.org

Tcharles V.B. Faria[1] ✉, Fernando J.S. Moreira[2]

[1]*Graduate Program in Electrical Engineering, Federal University of Minas Gerais, Belo Horizonte, MG 31270-901, Brazil*
[2]*Departament of Electronics Engineering, Federal University of Minas Gerais, Belo Horizonte, MG 31270-901, Brazil*
✉ *E-mail: tcharlesdefaria@ufmg.br*

Abstract: This work presents a new technique for the geometrical optics (GO) shaping of axisymmetric dual-reflector antennas. Both reflectors' generatrices are shaped by the continuous concatenation of conic sections, suited to provide simultaneous control of amplitude and phase of the aperture's GO field. With amplitude and phase control of the aperture field, the antenna designer has more options to achieve prescribed circularly symmetric radiation patterns. The GO formulation is derived for the well-known shaped Cassegrain configuration, but it can be easily adapted to other axisymmetric geometries. Illustrative GO designs are investigated and results validated by a full-wave analysis provided by the method of moments.

1 Introduction

In high-performance wireless communication systems, the use of shaped dual-reflector antennas may be an important option. Reflector shaping techniques have been investigated for quite a long time [1]. Most of them are based on the solution of ordinary differential equations (ODEs) [2] or assume a uniform phase distribution over the main-reflector aperture [3]. In order to avoid the numerical evaluation of ODEs, Kim and Lee [4] proposed a technique where the reflectors' generatrices are represented (and shaped) by the consecutive concatenation of conic sections. The technique not only avoids the solution of ODEs, but also enforces Snell's law and the conservation of energy throughout the bundle of rays departing from the optical focus where the feed phase centre is assumed to be. However, by using rectangular coordinates to analytically represent conic sections, the technique ended up based on a set of non-linear equations to be numerically solved. This problem was circumvented by Moreira and Bergmann [5], who used polar equations to represent the conic sections, thus solving the problem with a simple set of linear equations for each iteration of the geometrical optics (GO) shaping procedure. The shaping technique based on conic sections proved to be more numerically stable and robust than traditional methods based on ODEs [5]. Furthermore, the formulation was extended to shape omnidirectional dual-reflector geometries in [6].

Nevertheless, the authors of [4, 5] used parabolas to represent the main-reflector generatrix, thus achieving dual-reflector configurations where the aperture's field amplitude can be controlled, but the phase distribution is uniform. In this paper, the authors formulate an extension of the GO shaping procedure developed in [5], where the main-reflector generatrix is locally described by ellipses instead of parabolas. This allows the simultaneous control of the field's amplitude and phase at the main-reflector aperture, allowing more options for dual-reflector antenna designs with prescribed circularly symmetric radiation patterns. Another important feature of the new technique is that it can be easily adapted to shape any axisymmetric dual-reflector antenna belonging to the Axis-Displaced Cassegrain (ADC-like), Gregorian (ADG-like), Ellipse (ADE-like), and Hyperbola (ADH-like) configurations [7].

This paper is the full-version of [8]. In Section 2, the GO formulation to shape axisymmetric dual-reflector antennas with simultaneous amplitude and phase control is derived in detail for an ADC-like configuration. In Section 3, the shaping formulation is extended to an ADE-like antenna. To illustrate the applicability of the proposed technique, Section 4 presents the design of ADC- and ADE-like geometries, shaped to obtain desired radiation patterns according the amplitude and phase specifications over the main-reflector aperture. Two new case studies were included: a shaped ADE-like antenna with uniform phase (Section 4.1) and a shaped ADC-like configuration with a non-uniform phase distribution (Section 4.2). As the reflectors are shaped according to GO principles, full-wave analyses based on the method of moments (MoM) [9] are conducted to simulate the antennas' radiation patterns and verify the usefulness of the present technique.

2 Formulation of the GO shaping technique

The present dual-reflector antennas are composed of two circularly symmetric (i.e. bodies of revolution) reflecting surfaces with a common symmetry axis (z-axis). The main aspect of the shaping technique investigated here is the local representation of the reflectors' shaped generatrices by conic sections (namely ellipses and hyperbolas), which are continuously concatenated to provide, under GO principles, a prescribed field distribution over the main-reflector aperture, as illustrated in Fig. 1. Differently from [4, 5], in this work, the elliptical sections are employed to locally describe the main-reflector generatrix in order to simultaneously control the amplitude and phase of the aperture's field. In this section, the formulation is initially derived for an ADC-like configuration (see Figs. 1 and 2), and then adapted to ADE-like geometries in Section 3.

The shaped subreflector generatrix is sequentially described by conic sections S_n, with $n = 1, 2,\ldots, N$ (see Fig. 1). Each S_n has two foci: one always placed at the coordinate-system origin O (where the feed phase centre is assumed to be) and another at P_n [5]. For an ADC-like geometry P_n is virtual, as shown in Figs. 1 and 2; but for other configurations it may be real. The focus P_n, after the generatrix rotation around its symmetry axis, defines a local circular caustic for that subreflector portion. Furthermore, the main-reflector generatrix is describe by local ellipses M_n (with $n = 1, 2,\ldots, N$, as shown in Fig. 1), and each one of them has one focus coinciding with P_n and the other (T_n) at the main-reflector aperture. The location of T_n is known a priori and is related to prescribed aperture's amplitude and phase distributions.

The feed, with its phase centre at O, radiates a circularly-symmetric power density $G_F(\theta_F)$, where θ_F is the angle between the feed-ray and the z-axis. The rays emanating from O are reflected by S_n and M_n before arriving at T_n (see Fig. 2). The total optical path length ℓ_n from O to T_n is known a priori and related to the

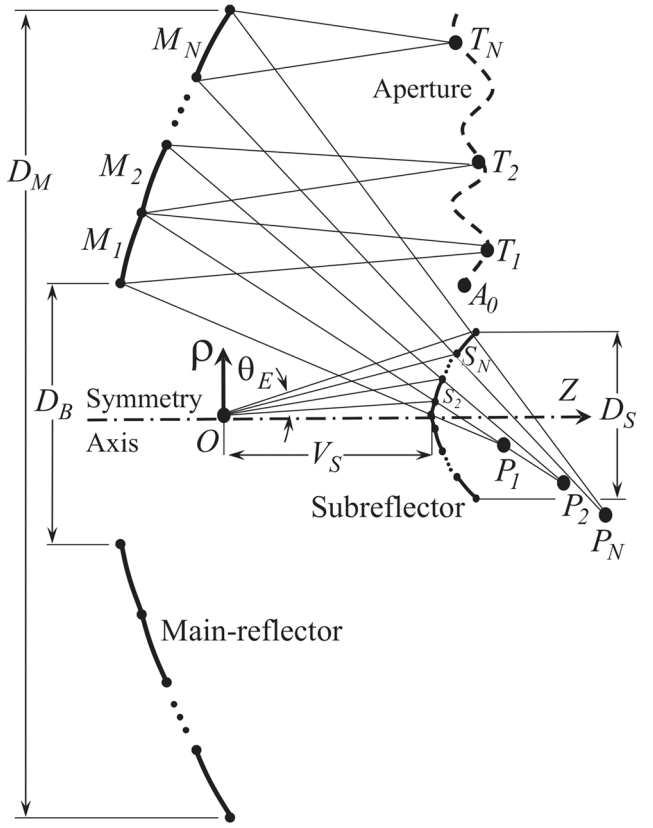

Fig. 1 *Dual-reflector antenna shaping by consecutive concatenation of local conic sections for an ADC-like configuration*

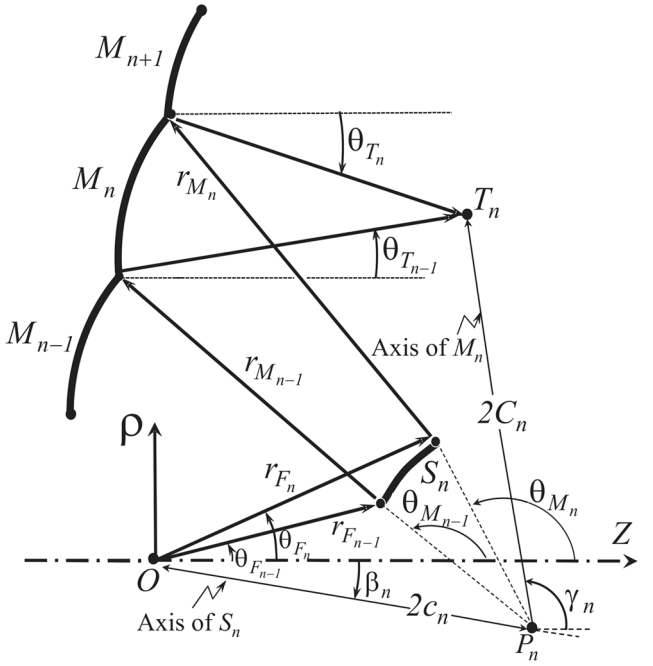

Fig. 2 *Parameters of the confocal conic sections S_n and M_n*

prescribed field's phase $k\ell_n$ at T_n, where k is the usual propagation constant. The prescribed field's amplitude at T_n is related to the energy conserved in the bundle of rays limited by S_n and M_n. As $N \to \infty$ one should have no problem in observing that the present concept is reasonable. However, the present shaping technique is based on a finite N and further MoM simulations will illustrate the usefulness of the procedure in Section 4.

The main-reflector aperture is defined by a set of points T_n, as shown in Fig. 1, located a priori by

$$z_{T_n}\hat{z} + \rho_{T_n}\hat{\rho}, \tag{1}$$

where z_{T_n} and ρ_{T_n} are the coordinates of T_n. It should be emphasised that the location of T_n is arbitrary, allowing any desired phase distribution at the aperture, in principle. For an ADC geometry (Fig. 1), the aperture description starts at A_0 with $\rho = D_B/2$, where D_B is the blockage diameter of the aperture.

In order to uniquely define the pair of conics S_n and M_n, six parameters must be determined for each iteration n (see Fig. 2). The subreflector section S_n delimited by $\theta_{F_{n-1}} \le \theta_F \le \theta_{F_n}$ is characterised by the following parameters: interfocal distance $2c_n$ (i.e. the distance between O and P_n), eccentricity e_n, and tilt angle β_n of its axis with respect to the z-axis. The corresponding main-reflector section M_n, delimited by $\theta_{M_{n-1}} \le \theta_M \le \theta_{M_n}$, is defined by its interfocal distance $2C_n$ (between P_n and T_n), eccentricity ϵ_n (with $0 < \epsilon_n < 1$ for an ellipse), and tilt angle γ_n with respect to the z-axis. Consequently, six equations are required to uniquely solve the shaping problem at each step n.

From the polar equation of a conic section [5], the following relation is obtained for S_n:

$$r_F(\theta_F) = \frac{a_n(\eta_F^2 + 1)}{b_n(\eta_F^2 - 1) + 2\eta_F d_n - (\eta_F^2 + 1)}, \tag{2}$$

where r_F is the distance from O to the subreflector and $\eta_F = \cot(\theta_F/2)$. For $\theta_{F_{n-1}} \le \theta_F \le \theta_{F_n}$:

$$a_n = c_n(e_n - 1/e_n), \tag{3}$$

$$b_n = e_n \cos\beta_n, \tag{4}$$

$$d_n = e_n \sin\beta_n. \tag{5}$$

Likewise, for M_n:

$$r_M(\theta_M) = \frac{A_n(\eta_M^2 + 1)}{B_n(\eta_M^2 - 1) + 2\eta_M D_n - (\eta_M^2 + 1)}, \tag{6}$$

where r_M is the distance from P_n to the main reflector and $\eta_M = \cot(\theta_M/2)$. For $\theta_{M_{n-1}} \le \theta_M \le \theta_{M_n}$:

$$A_n = C_n(\epsilon_n - 1/\epsilon_n), \tag{7}$$

$$B_n = \epsilon_n \cos\gamma_n, \tag{8}$$

$$D_n = \epsilon_n \sin\gamma_n. \tag{9}$$

Other important equations obtained for the confocal conics are the angular relations between θ_F, θ_M, and θ_T along the limited bundle of rays (see Fig. 2). From the polar equations of S_n and M_n one can show that

$$\eta_M = \frac{b_n - d_n\eta_F + 1}{d_n + \eta_F(b_n - 1)} \tag{10}$$

and

$$\eta_T = \cot\left(\frac{\theta_T}{2}\right) = \frac{g_1 - g_3 + \eta_F(1 + g_2 - g_4)}{1 - g_2 + \eta_F(g_1 + g_3) - g_4}, \tag{11}$$

where

$$g_1 = D_n - d_n, \tag{12}$$

$$g_2 = B_n - b_n, \tag{13}$$

$$g_3 = d_n B_n - b_n D_n, \tag{14}$$

$$g_4 = b_n B_n + d_n D_n . \tag{15}$$

For each step n, the shaping procedure is based on the energy conservation within the bundle of rays limited by $\theta_{F_{n-1}} \le \theta_F \le \theta_{F_n}$. With $\theta_{F_{n-1}}$ known from the previous step, θ_{F_n} is determined from

$$\int_{\theta_{F_{n-1}}}^{\theta_{F_n}} G_F(\theta_F) r_F^2 \sin\theta_F \mathrm{d}\theta_F = L_F P_{T_n}, \tag{16}$$

where $G_F(\theta_F)$ is the radiated feed power density, P_{T_n} is the desired power distribution at T_n, and

$$L_F = \frac{\int_0^{\theta_E} G_F(\theta_F) r_F^2 \sin\theta_F \mathrm{d}\theta_F}{\left(\sum_{n=1}^{N} P_{T_n}\right)} . \tag{17}$$

L_F is a normalisation factor ensuring that all feed power intercepted by the subreflector is conserved at the main-reflector aperture. The shaping procedure starts at $n = 1$ and ends at $n = N$ with $\theta_{F_N} = \theta_E$, the subreflector's edge angle. Theoretically, the accuracy of the algorithm increases as $N \to \infty$ [5].

The first shaping equation for step n comes from the conic relations of pair S_n, M_n. Noticing that these conic sections are confocal, one has

$$\ell_n = \frac{2c_n}{e_n} + \frac{2C_n}{\epsilon_n} . \tag{18}$$

Equation (18) is directly related to Malus' theorem for conics S_n and M_n. Notice that the path length ℓ_n, z_{T_n}, and ρ_{T_n} are known a priori. The second equation is obtained with the help of Fig. 2

$$2C_n = \sqrt{(2c_n\cos\beta_n - z_{Tn})^2 + (2c_n\sin\beta_n - \rho_{T_n})^2} . \tag{19}$$

The third equation of step n is derived from simple trigonometric relations involving γ_n. With the help of Fig. 2, one obtains

$$\sin\gamma_n = \frac{\rho_{T_n} - 2c_n\sin\beta_n}{2C_n}, \quad \cos\gamma_n = \frac{z_{T_n} - 2c_n\cos\beta_n}{2C_n} . \tag{20}$$

Then, from (8), (9), and (20), the third equation is obtained

$$\frac{D_n}{B_n} = \frac{\rho_{T_n} - 2c_n\sin\beta_n}{z_{T_n} - 2c_n\cos\beta_n} . \tag{21}$$

Noticing that both $\theta_{F_{n-1}}$ and $r_{F_{n-1}}$ are known from the previous step, the fourth equation is obtained from (2)

$$r_{F_{n-1}} = \frac{a_n(\eta_{F_{n-1}}^2 + 1)}{b_n(\eta_{F_{n-1}}^2 - 1) + 2\eta_{F_{n-1}} d_n - (\eta_{F_{n-1}}^2 + 1)}, \tag{22}$$

where $\eta_{F_{n-1}} = \cot(\theta_{F_{n-1}}/2)$. For the first step, $\theta_{F_0} = 0$ and $r_{F_0} = V_S$ is the distance between the feed phase centre and the subreflector vertex, known a priori.

The remaining two equations are determined with the help of the angular mapping $\theta_F \to \theta_T$, given by (11). Applying simple trigonometric relations and with the help of Fig. 2, one can obtain relations between the main-reflector ρ coordinates from steps $n-1$ and n and the ρ coordinate ρ_{T_n} of focus T_n. The resulting equations are

$$\begin{aligned} &r_{M_{n-1}}(\sin\theta_{M_{n-1}} - \sin\theta_{T_{n-1}}) + \frac{2C_n}{\epsilon_n}\sin\theta_{T_{n-1}} + 2c_n\sin\beta_n \\ &= \rho_{T_n}, \end{aligned} \tag{23}$$

$$r_{M_n}(\sin\theta_{M_n} - \sin\theta_{T_n}) + \frac{2C_n}{\epsilon_n}\sin\theta_{T_n} + 2c_n\sin\beta_n = \rho_{T_n}, \tag{24}$$

where η_M and η_T are given in terms of η_F by (10) and (11), respectively, while $r_{M_{n-1}}$ and r_{M_n} are given by (6) with $\theta_F = \theta_{F_{n-1}}$ and θ_{F_n}, respectively.

Equations (22)–(24) form a set of three non-linear equations, which must be numerically solved to obtain the parameters $2c_n$, e_n, and β_n of S_n. Afterwards, the parameters of M_n are obtained as follows. $2c_n$, e_n, and β_n are substituited into (3)–(5) to obtain a_n, b_n, and d_n. Then, $2C_n$ and ϵ_n are calculated with the help of (19) and (18), respectively. Finally, γ_n is determined from (21). Once, $2C_n$, ϵ_n, and γ_n are known, A_n, B_n, and D_n are readily calculated from (7)–(9).

With all parameters of S_n and M_n determined, the shaped subreflector point at $\theta_F = \theta_{F_n}$ is located by

$$r_{F_n}\cos\theta_{F_n}\hat{z} + r_{F_n}\sin\theta_{F_n}\hat{\rho}, \tag{25}$$

while its main-reflector counterpart is located by

$$(r_{M_n}\cos\theta_{M_n} + 2c_n\cos\beta_n)\hat{z} + (r_{M_n}\sin\theta_{M_n} + 2c_n\sin\beta_n)\hat{\rho} . \tag{26}$$

The iterations are repeated until $\theta_{F_N} = \theta_E$ for $n = N$.

3 GO shaping technique for an ADE-like geometry

The shaping formulation presented in Section 2 was derived for an ADC-like geometry, as depicted in Figs. 1 and 2. However, it can be easily adapted to consider other circularly symmetric configurations. In this section, the simple modifications needed to adapt the shaping procedure to an ADE-like geometry (see Fig. 3) is discussed. Notice that, for the present geometry, all foci P_n are real, thus indicating that the subreflector generatrix is now described by ellipses S_n. Nevertheless, the real foci P_n provide the inversion of the feed illumination toward the main-reflector aperture [5]. Consequently, one just needs to sort the aperture foci T_n in reverse order, i.e. from top to bottom according to the orientation shown in Fig. 3. So, now the main-reflector aperture starts at A_0 with $\rho = D_M/2$, where D_M is the projected main-reflector diameter. The remaining of the shaping procedure is kept the same as in Section 2.

4 GO shaping results

In order to demonstrate the GO shaping technique described in Sections 2 and 3, the designs of ADC- and ADE-like geometries are investigated in this section. Under GO principles, the reflectors were shaped to yield a pencil-beam or flat-topped radiation patterns, according to the amplitude and phase distributions specified over the main-reflector aperture. The shaped antennas' radiation patterns were simulated by rigorous full-wave analyses based on the numerical solution of a surface Electric Field Integral Equation (EFIE) using the MoM [9], to validate the GO shaping procedure. For all cases investigated in this section, the following circularly-symmetric raised cosine feed (RCF) model was adopted

$$G_F(\theta_F) = \frac{\cos^{2p}(\theta_F/2)}{2\eta_0 r_F^2} . \tag{27}$$

where η_0 is the free-space impedance and p controls the RCF pattern. To obtain θ_{F_n} from (16), the desired power distribution (P_{T_n}) over the main-reflector aperture is defined a priori as

$$P_{T_n} = \int_{\rho_{A_{n-1}}}^{\rho_{A_n}} G_A(\rho)\,\rho\,\mathrm{d}\rho, \tag{28}$$

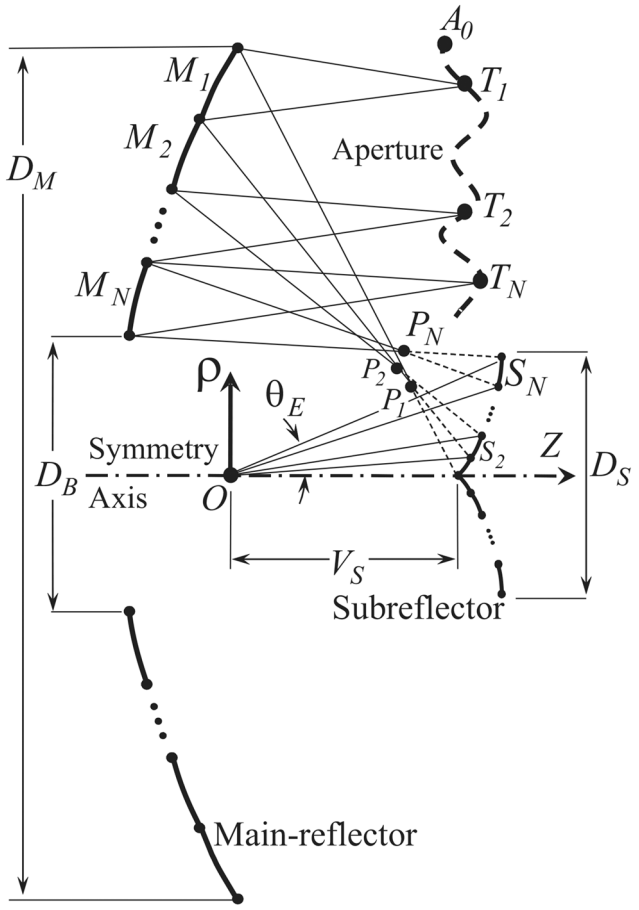

Fig. 3 *Dual-reflector antenna shaping by consecutive concatenation of local conic sections for an ADE-like configuration*

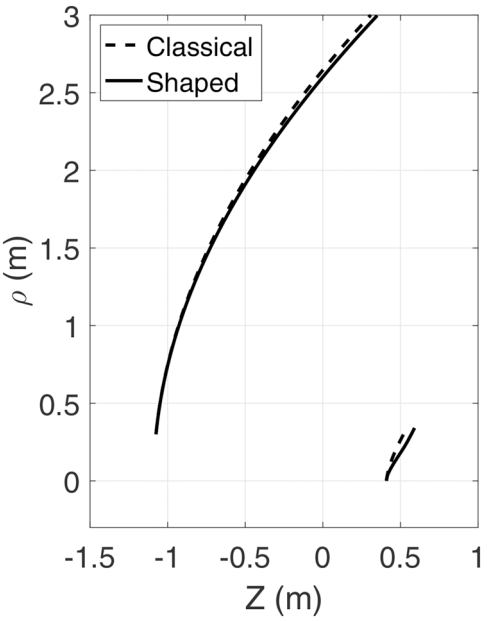

Fig. 4 *Sub- and main-reflectors' generatrices of the classical (dashed lines) and shaped (solid lines) ADC configurations*

with focus T_n lying between aperture points with ρ coordinates $\rho_{A_{n-1}}$ and ρ_{A_n}, while $G_A(\rho)$ is the prescribed aperture power density.

4.1 ADC- and ADE-like configurations shaped with uniform phase distribution

In this section, the reflectors of ADC and ADE antennas are shaped with uniform phase distribution at the main-reflector aperture, in order to compare results with those of [5] and establish the

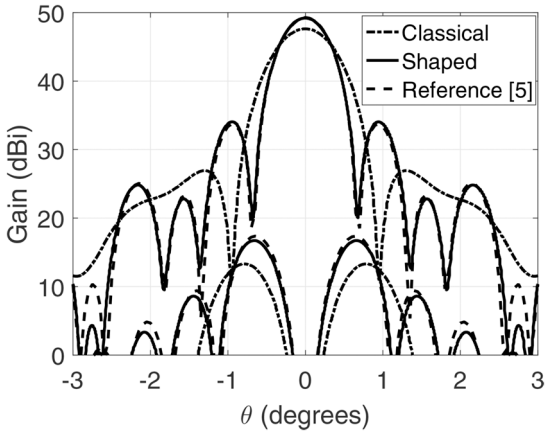

Fig. 5 *MoM Co- and Cx-polarisation patterns of the shaped ADC configuration (solid lines), together with those of the classical configuration (dash-dotted lines) and the shaped geometry of [5] (dashed lines)*

functionality of the present shaping technique. Furthermore, in both case studies, the main-reflector aperture is planar, with z_{T_n} and ℓ_n both constants, providing radiation patterns with the highest gain at boresight ($\theta = 0$).

Following a case study previously investigated in [4, 5], in the first example, an ADC-like antenna was shaped to provide a uniform aperture illumination (i.e. both amplitude and phase are constants at the aperture). As in [5], the shaping departed from a classical geometry [7] with $D_M = 100\lambda$, $D_B = D_S = 10\lambda$, $\theta_E = 30°$, and $\ell_0 = 50\lambda$, assuming a planar aperture at $z = 0$. Consequently, the distance from O to the subreflector vertex was established as $V_S = 6.81\lambda$. The reflectors' generatrices of the classical ADC are illustrated with dashed lines in Fig. 4. The procedure described in Section 2 was then employed with constant $G_A(\rho)$ and $\ell_n = \ell_0$. The aperture foci T_n were uniformly distributed between $\rho_{A_0} = D_B/2$ and $\rho_{A_N} = D_M/2$. The RCF model was that of (27) with $p = 83$ to provide -25 dB edge taper [4, 5]. The iterative procedure started with $\theta_{F_0} = 0$ and $r_{F_0} = V_S$. The analyses where conducted at 5 GHz, where, for instance $D_M = 6$ m and $D_B = D_S = 0.6$ m.

The reflectors' generatrices of the shaped ADC are shown with solid lines in Fig. 4, together with the initial classical geometry. The MoM radiation patterns of the classical and shaped (with $N = 1000$) ADC antennas are shown in Fig. 5 at the diagonal plane $\phi = 45°$, together with the radiation pattern of the antenna shaped in [5]. The simulations indicate a shaped antenna with a gain of 49.2 dBi, which is 1.4 dB higher than that of the classical configuration. Also, the shaped ADC has a cross-polarisation ~ 5 dB higher than the classical geometry. From Fig. 5 one observes that the results obtained by the present shaping procedure show an excellent agreement with those of [5].

In the second case study, an ADE-like antenna was shaped to provide a tapered aperture illumination, as in [5], with $D_M = 20\lambda$, $D_B = D_S = 3.23\lambda$, $\theta_E = 45°$, and $\ell_0 = 10.32\lambda$ (with $z_A = 0$). These geometrical parameters provided an initial classical ADE configuration with $V_S = 1.17\lambda$ [7]. Following [5], the RCF of (27) was used once more, but now with $p = 23.5$.

Instead of a uniform illumination, the aperture's amplitude was tapered as [5]:

$$G_A(\rho) = 1 - (1 - E_M^2)\left(\frac{2\rho_A - D_B}{D_M - D_B}\right)^2, \tag{29}$$

with $E_M = 0.6$ [5]. The aperture foci T_n were uniformly distributed between $\rho_{A_0} = D_M/2$ and $\rho_{A_N} = D_B/2$, now in the reverse order. The analyses were conducted at 14.7 GHz, where, for instance $D_M = 40.64$ cm and $D_B = D_S = 6.6$ cm. Fig. 6 shows the sub- and main-reflectors' generatrices of the classical (dashed lines) and shaped (solid lines) ADE antennas. The MoM radiation patterns at

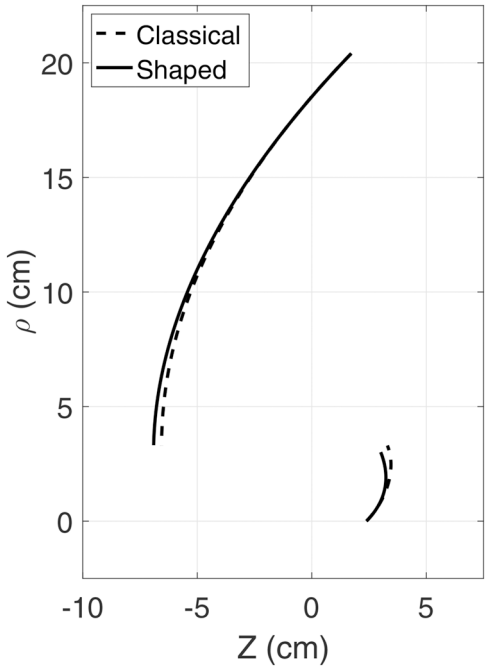

Fig. 6 *Sub- and main-reflectors' generatrices of the classical (dashed lines) and shaped (solid lines) ADE configurations*

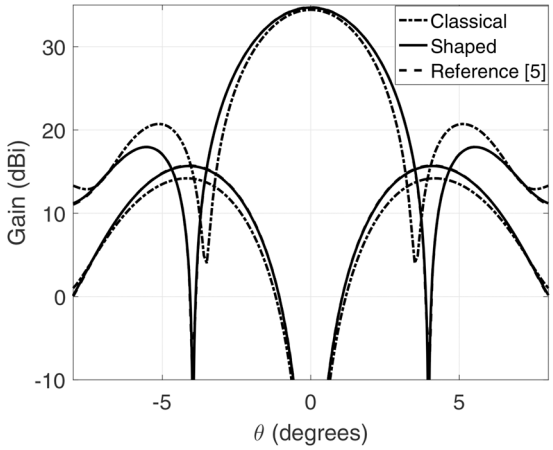

Fig. 7 *MoM Co- and Cx-polarisation patterns of the shaped ADE configuration (solid lines), together with those of the classical configuration (dash-dotted lines) and the shaped geometry of [5] (dashed lines)*

$\phi = 45°$ for the classical and shaped (with N = 1000) configurations are shown in Fig. 7, together with the pattern of the shaped antenna of [5]. From Fig. 7 one observes that the results obtained by the present shaping procedure show an excellent agreement with those of [5], proving once again the effectiveness of the present technique. The MoM analyses indicated a slight increase of the gain of the shaped antenna, from 34 dBi to 34.4 dBi, together with a more significant decrease of the sidelobe levels, as expected.

4.2 ADC-like configuration shaped with a non-uniform phase distribution

In this section, the reflectors' generatrices of an ADC-like antenna are shaped with a non-uniform aperture illumination, providing simultaneous control of amplitude and phase distributions. For the present case study, the main-reflector aperture remained planar (i.e. with constant z_{T_n}), but with the several ℓ_n varied according to the desired phase specification. The adopted amplitude and phase distributions were based on those investigated in [10] to provide a flat-topped radiation pattern. Figs. 8 and 9 illustrate the continuous

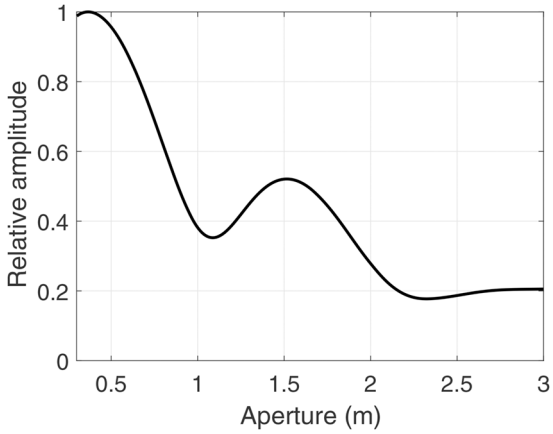

Fig. 8 *Relative amplitude distribution of [10]*

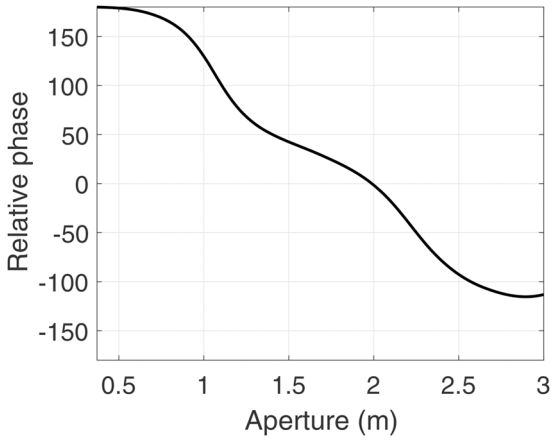

Fig. 9 *Relative phase distribution of [10]*

versions of the amplitude and phase distributions adopted in the shaping procedure, respectively.

For comparison purposes, the initial parameters used in the shaping procedure were those of the classical ADC of the previous subsection, with $D_M = 100\lambda$, $D_B = D_S = 10\lambda$, $\theta_E = 30°$, and $V_S = 6.81\lambda$. The RCF of (27) was employed with $p = 83$. Once again, foci T_n were uniformly distributed between $\rho_{A_0} = D_B/2$ and $\rho_{A_N} = D_M/2$. The shaped generatrices (in solid lines) are shown in Fig. 10, together with the classical ADC configuration (dashed lines) already shown in Fig. 4. MoM radiation patterns of the shaped ADC antenna (using $N = 400$) in the E-plane ($\phi = 90°$) are shown in Fig. 11 at 4 GHz (with $D_M = 80\lambda$) and 5 GHz ($D_M = 100\lambda$). The non-uniform illumination of Figs. 8 and 9 almost provided the desired flat-topped radiation pattern. Differently from [10], here the aperture's blockage imposed by the subreflector yielded ripples in the main lobe. As frequency is increased up to 5 GHz, the radiation pattern tends to be more directive, as expected. Due to the aperture's amplitude tapering, sidelobe levels are relatively small (about 20 dB below at both frequencies).

5 Conclusion

A new GO shaping of axisymmetric dual-reflector antennas has been presented. Sub- and main reflectors' generatrices were shaped by the continuous concatenation of local conic sections in order to provide simultaneous control of field amplitude and phase over the main-reflector aperture. The formulation was derived for ADC- and ADE-like antennas, but it can be easily adapted to other circularly-symmetric dual reflector geometries.

In other to demonstrate the usefulness of the proposed technique, ADC- and ADE-like antennas with uniform phase distributions were synthesised and results were successfully compared to those in the literature [5]. As the shaping technique is based on the GO principles, rigorous full-wave analyses based on

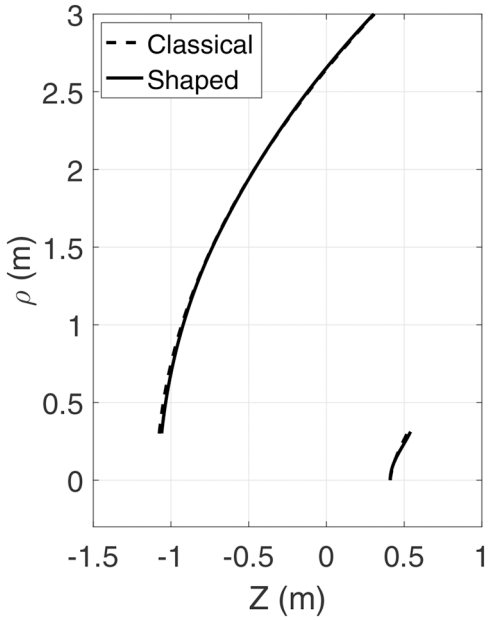

Fig. 10 *Sub- and main-reflectors' generatrices of the shaped (classic lines) and uniform aperture (dashed lines) ADC configurations*

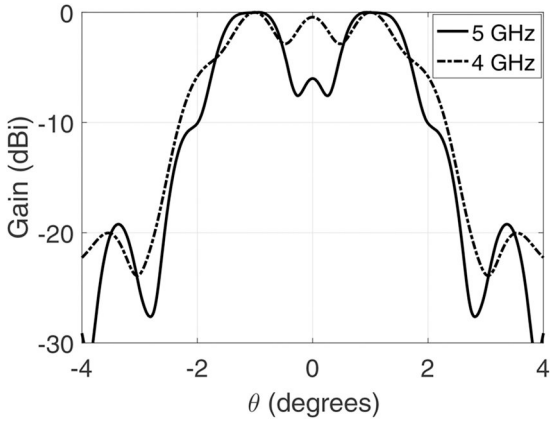

Fig. 11 *MoM radiation patterns of the shaped ADC configuration at 5 GHz (solid lines) and 4 GHz (dashed lines)*

the MoM were conducted to simulate the antennas' radiation patterns and verify the effectiveness of the GO syntheses. Finally, an ADC-like configuration was successfully designed to provide a flat-topped radiation pattern by simultaneously controlling the aperture's amplitude and phase distributions.

6 Acknowledgments

This work was supported by the Brazillian agencies CAPES, CAPES/PROCAD 068419/14 and CNPq.

7 References

[1] Kimber, B.Y.: 'On two reflector antennas', *Radio Eng. Electron. Phys.*, 1962, **6**, pp. 914–921

[2] Galindo, V.: 'Design of dual-reflector antennas with arbitrary phase and amplitude distributions', *IEEE Trans. Antennas Propag.*, 1964, **12**, (4), pp. 403–408

[3] Lee, J.J., Parad, L.I., Chu, R.S.: 'A shaped offset-fed dual-reflector antennas', *IEEE Trans. Antennas Propag.*, 1979, **27**, (2), pp. 165–171

[4] Kim, Y., Lee, T.-H.: 'Shaped circularly symmetric dual reflector antennas by combining local conventional dual reflector systems', *IEEE Trans. Antennas Propag.*, 2009, **57**, (1), pp. 47–56

[5] Moreira, F.J.S., Bergmann, J.R.: 'Shaping axis-symmetric dual-reflector antennas by combining conic sections', *IEEE Trans. Antennas Propag.*, 2011, **59**, (3), pp. 1042–1046

[6] Penchel, R.A., Zang, S.R., Bergmann, J.R., *et al.*: 'GO shaping of omnidirectional dual-reflector antennas with arbitrary main-beam direction in elevation plane by connecting conic sections', *Int. J. Antennas Propag.*, 2018, **2018**, pp. 1–9, ID 1409716

[7] Moreira, F.J.S., Prata, A. Jr.: 'Generalized classical axially symmetric dual-reflector antennas', *IEEE Trans. Antennas Propag.*, 2001, **49**, (4), pp. 547–554

[8] Faria, T.V.B., Moreira, F.J.S.: 'A new technique for shaping axis-symmetric dual-reflector antennas using conic sections'. Proc. SBMO/IEEE MTT-S Int. Microwave and Optoelectronics Conf., Aveiro, Portugal, November 2019, pp. 1–3

[9] Moreira, F.J.S.: 'Design and rigorous analysis of generalized axially-symmetric dual-reflector antennas'. PhD Thesis, Dept. Electrical Engineering–Electrophysics, University of Southern California, Los Angeles, USA, August 1997

[10] Elliot, R.S., Stern, G.J.: 'Shaped patterns from a continuous planar aperture distribution', *IEE Proc. H - Microwaves, Antennas Propag.*, 1988, **135**, (6), pp. 366–370